SHIP-BOARD MEASUREMENTS AND ESTIMATIONS OF AIR-SEA FLUXES IN THE WESTERN TROPICAL PACIFIC DURING TOGA COARE

XILONG SONG and CARL A. FRIEHE
Department of Mechanical and Aerospace Engineering, University of California, Irvine, CA 92697-3975, USA
DUNXIN HU
Institute of Oceanology, Chinese Academy of Sciences, Qingdao 266071, P. R. China

(Received in final form 28 June, 1996)

Abstract. Direct air-sea flux measurements were made on R/V Kexue #1 at 4° S, 156° E during the Tropical Ocean Global Atmosphere (TOGA) Coupled Ocean-Atmospheric Response Experiment (COARE) Intensive Observation Period (IOP). An array of six accelerometers was used to measure the motion of the anchored ship, and a sonic anemometer and Lyman-α hygrometer were used to measure the turbulent wind vector and specific humidity. The contamination of the turbulent wind components by ship motion was largely removed by an improvement of a procedure due to Shao based on the acceleration signals. The scheme of the wind correction for ship motion is briefly outlined. Results are presented from data for the best wind direction relative to the ship to minimize flow distortion effects. Both the time series and the power spectra of the sonic-measured wind components show swell-induced ship motion contamination, which is largely removed by the accelerometer correction scheme. There was less contamination in the longitudinal wind component than in the vertical and transverse components. The spectral characteristics of the surface-layer turbulence properties are compared with those from previous land and ocean results. Momentum and latent heat fluxes were calculated by eddy correlation and compared to those estimated by the inertial dissipation method and the TOGA COARE bulk formula. The estimations of wind stress determined by eddy correlation are smaller than those from the TOGA COARE bulk formula, especially for higher wind speeds, while those from the bulk formula and inertial dissipation technique are generally in agreement. The estimations of latent heat flux from the three different methods are in reasonable agreement. The effect of the correction for ship motion on latent heat fluxes is not as large as on momentum fluxes.

Key words: TOGA COARE, Wind correction for ship motion, Air-sea fluxes

1. Introduction

Accurate parameterizations of air-sea sensible, latent heat and momentum fluxes are important in air-sea interaction. Coupled ocean-atmospheric global climate models require an accuracy of ± 10 Wm^{-2} of the net surface heat flux for the prediction of climate change (cf. Webster and Lukas, 1992). Miller *et al.* (1992) found that large changes in European Center for Medium-Range Weather Forecasts (ECMWF) model outputs were caused by adjusting the flux parameterizations in the western Pacific warm pool region. The Tropical Ocean Global Atmosphere Coupled Ocean-Atmosphere Experiment, TOGA COARE, was designed to study the meteorology, oceanography and air-sea interaction in the warm pool region. The measurement of air-sea fluxes and their parameterizations is one of the major

Boundary-Layer Meteorology **81:** 373–397, 1996.

goals of TOGA COARE (Webster and Lukas, 1992). By definition the fluxes are the ensemble Reynolds averages of the instantaneous vertical air velocity component with horizontal momentum, enthalpy and water vapor density to give the stress, sensible heat flux and latent heat flux, respectively. The so-called eddy-correlation method is the definitive method to determine the surface fluxes, but it requires measurements of the vertical and downwind components of air velocity, temperature and humidity over a sufficiently long averaging period and with sufficient frequency response. Such measurements are complicated by the contamination of anemometer signals due to platform motion. The crucial part of the measurement of the wind vector for turbulent flux computations from a ship is the removal of the ship motion from the measured wind vector (Mitsuta and Fujitani, 1974). Since the ship is, in general, free to rotate and accelerate, the three orientation angles and three velocity components of its motion have to be measured. As a result, direct flux measurements over the deep oceans are not as easy and frequent as they are over land, though some good observations have been made recently, for instance, on a ship by Bradley *et al.* (1991) and on a buoy by Anctil *et al.* (1993). Different methods have been used to measure platform (ship or buoy) motion. One of the systems used successfully is a combination of a vertical gyro and accelerometers (Fujitani, 1985; Tsukamoto *et al.*, 1990). A similar method was used on a buoy by Anctil *et al.* (1993) for measuring the buoy orientation (roll, pitch and yaw angles). Tsukamoto and Ishida (1995) used a high-precision gyro and three accelerometers to measure the three velocity components and angles of the ship on the R/V Hakuhomaru during TOGA COARE. However, other investigators have used similar systems, but encountered considerable practical difficulties caused possibly by the inadequate intrinsic damping of the gyro system and reported only minor success (Bradley *et al.* 1991). Bradley *et al.* (1991) used a system of six accelerometers which were arranged in three pairs in order to measure the 3-dimensional accelerations of the ship. The system, theory and numerical analysis scheme were described by Shao (1995). More sophisticated instruments with potential application in measuring the ship motion, such as differential GPS (Global Positioning System), are becoming available. A differential GPS system combined with 9 accelerometers was used on R/V Franklin during the TOGA COARE field experiment (Bradley and Weller, 1995), but there are still problems using differential GPS system for measuring ship motion (Bradley, 1996, personal communication).

Ship-board flux systems were deployed in the TOGA COARE Intensive Observation Period (IOP), which was conducted from November 1, 1992 through February 28, 1993 in the western tropical Pacific ocean where the sea surface temperature (SST) is the highest for all the world oceans. During the IOP, 14 ships were used to make meteorological and oceanic observations. R/V Kexue #1 from the Institute of Oceanology, Chinese Academy of Sciences, was located at the south apex (4° S, 156° E) of the Intensive Flux Array (IFA) (Figure 1) for almost the whole IOP. It was anchored on-station for three periods: 10 November–12 December 1992, 19 December 1992–23 January 1993 and 1 February–20 February 1993. Occasionally,

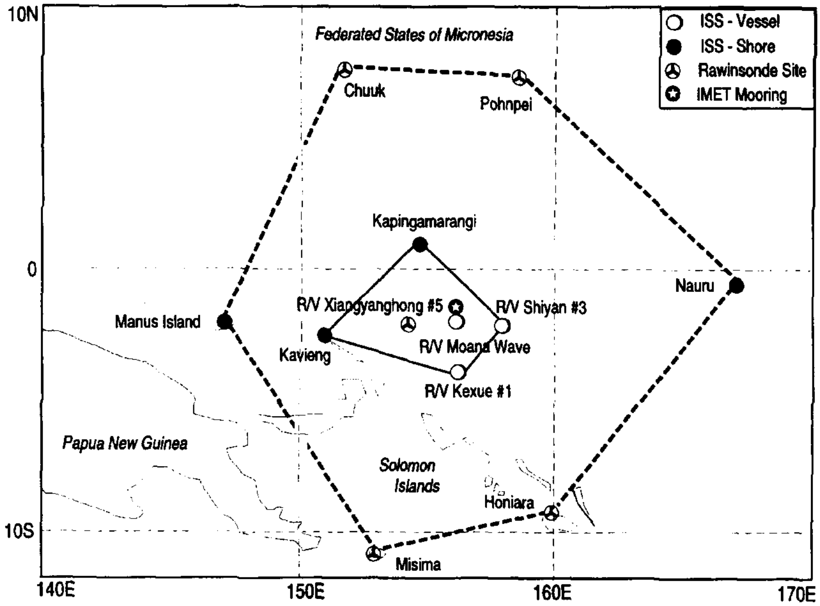

Figure 1. Map of the Intensive Flux Array (IFA) in the TOGA COARE domain.

the ship lost its anchor and drifted slowly, but moved back to its nominal position (4° S, 156° E) once a day.

Observations made on R/V Kexue #1 included integrated sounding system (ISS), conventional surface meteorology, direct air-sea fluxes, and conductivity-temperature-depth (CTD), and acoustic Doppler current profiler (ADCP) measurements of the ocean. A strap-down system of six accelerometers was used to measure the ship motion for the direct air-sea flux measurements. This installation has no gyros and is relatively inexpensive, which makes it suitable for long periods of operation at sea. Since an accelerometer cannot distinguish the true acceleration along its sensitive axis from the rotation in the Earth's gravitational field, six are needed to obtain the three components of acceleration and the three attitude angles. This paper describes the direct air-sea flux measurements on R/V Kexue #1 during TOGA COARE IOP and discusses surface-layer characteristics and flux estimations. The instrumentation and data acquisition are described in Section 2. In Section 3, the theory and corresponding numerical scheme of turbulent wind correction for ship motion are briefly outlined. Data processing results and analysis are shown in Section 4. Discussion and conclusions are presented in Section 5.

2. Instrumentation and Data Acquisition

The system on board R/V Kexue #1 for measuring air-sea fluxes was composed of a Kajio Denki model DAT-300 sonic anemometer-thermometer for measuring the

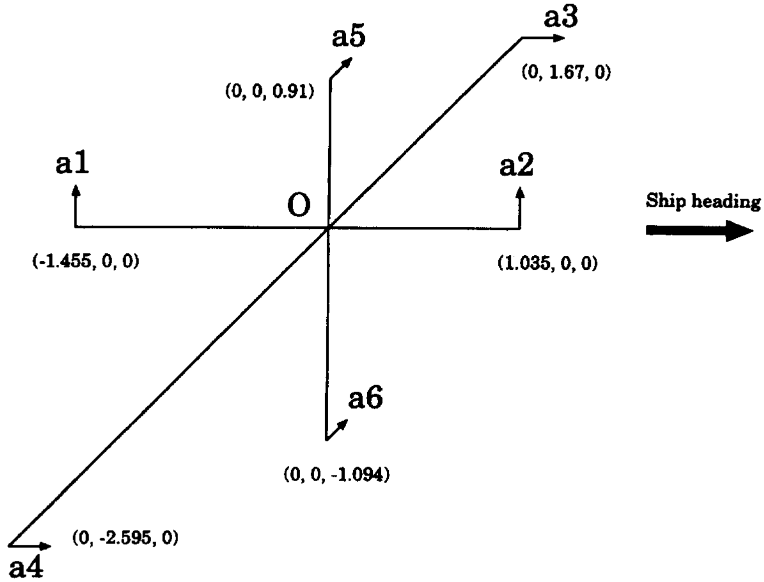

Figure 2. The six accelerometer system ($a1$, $a2$, $a3$, $a4$, $a5$, $a6$) for measuring ship motion used on R/V Kexue #1 during TOGA COARE. Coordinates from the origin (O) are in meters.

3-dimensional turbulent wind vector and the fluctuating virtual temperature, a Buck Lyman-α hygrometer for measuring the specific humidity fluctuations and six Q-Flex accelerometers for the determination of the ship motion and attitude. The sonic anemometer and Lyman-α were mounted on opposite ends of the crossarm (about 2 metres long) on the foremast (14 metres high above the water surface), while the six accelerometers were mounted in the forecastle just under the foremast on each of the four bulkheads, the ceiling and the floor, respectively, in three orthogonal pairs with two accelerometers of each pair along the same axis. Since an individual accelerometer responds only to the acceleration component in the direction of its axis, each pair of accelerometers measured only one component of acceleration. The three pairs of accelerometers were arranged such that one pair was towards the bow of the ship, one towards the port side and the other one vertically upward, measuring the longitudinal, lateral and normal acceleration components of the ship respectively. In addition, for the convenience of the numerical correction scheme, the three axes connecting the two accelerometers of each pair were joined at a common origin and formed a Cartesian system. The placement of the accelerometers is illustrated in Figure 2, where the notation is that accelerometers 1 and 2 are pointed upwards, measuring the normal acceleration component of the ship; accelerometers 3 and 4 are directed to bow, measuring the longitudinal acceleration component; while accelerometers 5 and 6 are directed to the port side of the ship, measuring the lateral acceleration component. The relative positions of the six accelerometers about the origin (in metres) are:

$$r_1 = (-1.455, 0, 0), \qquad r_2 = (1.035, 0, 0),$$

$$r_3 = (0, 1.67, 0), \qquad r_4 = (0, -2.595, 0),$$

$$r_5 = (0, 0, 0.91), \qquad r_6 = (0, 0, -1.094).$$

The relative position of the sonic sensor to the accelerometer origin is $R = (2.63$ m, -1.45 m, 12.23 m). All the instruments were calibrated before the cruise. The signals from the six accelerometers, the sonic anemometer-thermometer and Lyman-α were sampled at 10 Hz for 24 min data record periods. Usually the data records were made four times a day at local times 0400, 1000, 1600 and 2200.

There were also independent surface meteorological measurements from the ISS including wind speed, wind direction, barometric pressure, air temperature, relative humidity, shortwave and longwave radiation, with a time resolution of one min. The ISS sensors were mounted on the top of the main mast of the ship, which was about 60 metres aft of the foremast. In addition, conventional surface meteorological observations were also made on the upper deck at a height close to that of the sonic anemometer. These observations included hourly measurements of the five-minute mean wind vector, wet-bulb and dry-bulb temperatures, barometric pressure and shortwave and longwave radiation fluxes (both upward and downward). The sea-surface temperature (SST) was measured by a sensor attached to the ADCP which was about 4.5 m under the sea surface. The bulk meteorological time series is shown in Figure 3, for the hourly conventional meteorological measurements on the upper deck. The first period of the IOP is characterized by relatively low winds and rising SST which shows an obvious diurnal variation; the second by westerly wind burst with a decreasing SST, and the third by a weaker westerly wind burst and slightly decreasing SST.

3. Correction for Ship Motion

The correction of the wind vector contaminated by ship motion is based on the equation

$$\mathbf{V}_t = T\mathbf{V}_o' + \boldsymbol{\Omega} \times T\mathbf{R}' + \mathbf{V}_{sh}, \tag{1}$$

where $\mathbf{V}_t$ is the wind velocity corrected to Earth coordinates, $\mathbf{V}_o'$ the wind velocity observed in ship coordinates (i.e., the sonic anemometer output), $\boldsymbol{\Omega}$ the angular velocity of the ship in Earth coordinates, $\mathbf{R}'$ the position vector of the sonic anemometer expressed in ship coordinates, and $\mathbf{V}_{sh}$ the translational velocity of the ship body ($\mathbf{V}_{sh}$ is actually the velocity of the ship coordinate origin) in Earth coordinates, and T is the coordinate transformation matrix. Variables with primes are expressed in the ship coordinates while those without a prime are in Earth coordinates. For details of the ship and Earth coordinates, see the technical report

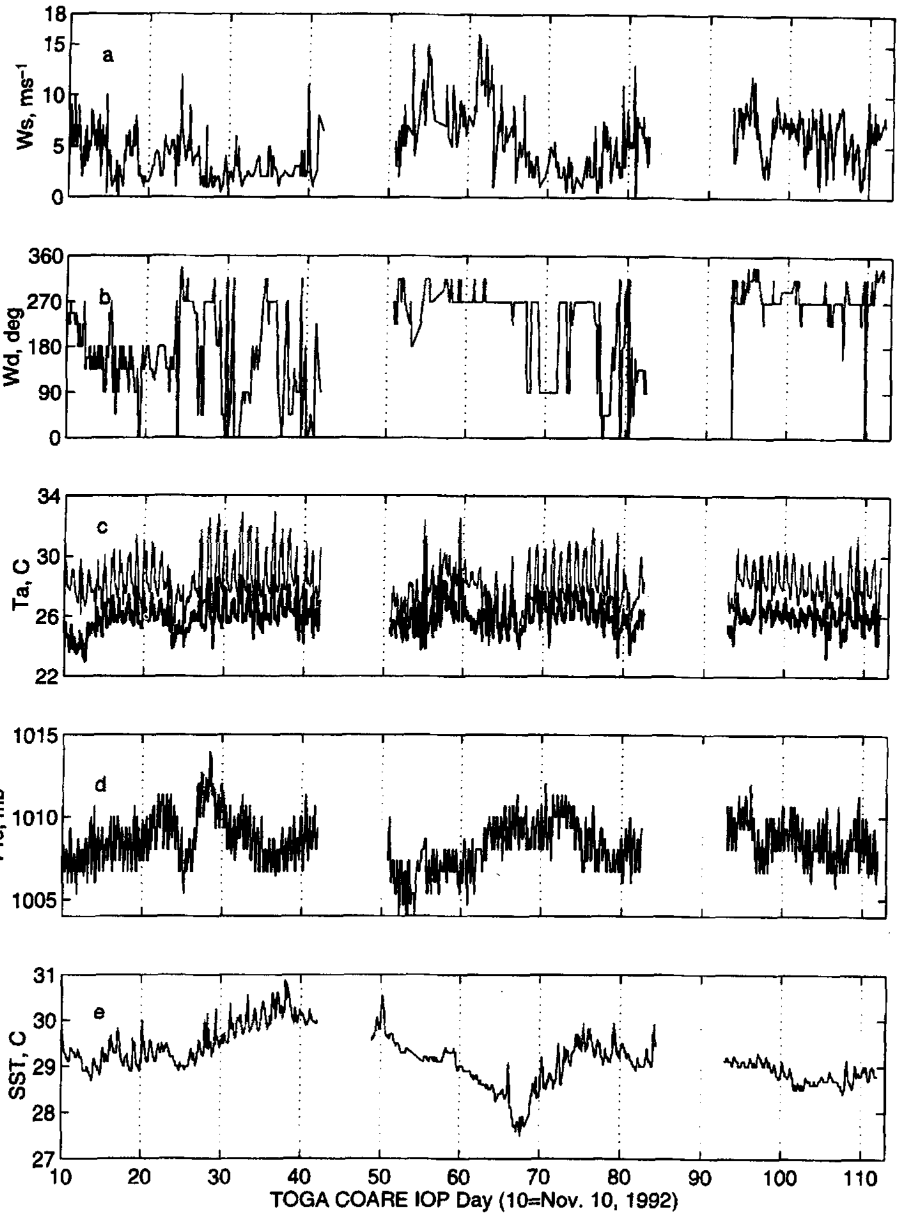

Figure 3. Hourly bulk meteorological measurements from R/V Kexue #1. (a) wind speed (ms^{-1}); (b) wind direction (degree); (c) dry bulb temperature (thin) and wet bulb temperature (thick) (°C); (d) barometric pressure (mb); and (e) sea surface temperature (°C). Gaps in the data are due to port calls.

by Shao (1995). All the vector variables can be expressed in component form as $\mathbf{V}_t = (u_t, v_t, w_t)$, $\mathbf{V}_{sh} = (u_{sh}, v_{sh}, w_{sh})$, $\mathbf{V}_o' = (u_o, v_o, w_o)$, $\mathbf{R}' = (R_x, R_y, R_z)$, where u, v and w are the velocity components in the longitudinal (x), lateral (y)

and vertical (z) directions, respectively. The angular velocity $\boldsymbol{\Omega} = (\dot{\phi}, \dot{\theta}, \dot{\psi})$, where ϕ, θ and ψ are the ship attitude angles of roll, pitch and yaw, respectively. The overhead dot indicates the time derivative.

This basic equation requires measurements of the angular velocity $\boldsymbol{\Omega}$, the translational velocity $\mathbf{V}_{sh}$ and the attitude angles of the ship, which determine the coordinate transformation matrix. If these quantities are directly measured, the correction of wind is rather straightforward in principle. In the method of Shao (1995), however, these quantities have to be obtained indirectly from the six accelerometer signals.

The velocity of an accelerometer ($\mathbf{V}_p$) referenced in Earth coordinates is related to the angular velocity ($\boldsymbol{\Omega}$) and the translational velocity ($\mathbf{V}_{sh}$) of the ship by

$$\mathbf{V}_p = \mathbf{V}_{sh} - T\mathbf{r}'_p \times \boldsymbol{\Omega}, \tag{2}$$

where $\mathbf{r}'_p$ is the position vector of the pth accelerometer from the origin of the ship coordinates (the origin of the accelerometers), $p = 1 \ldots 6$ specifying the positions of the six accelerometers. The inverse form of Equation (2) is

$$\mathbf{V}'_p = T^{-1}\mathbf{V}_{sh} + \boldsymbol{\Omega} \times \mathbf{r}'_p. \tag{3}$$

Based on this equation, the translational velocity of the ship $\mathbf{V}_{sh}$, the angular velocity $\boldsymbol{\Omega}$, and the attitude angles ϕ, θ and ψ can be obtained, since the vector $\mathbf{V}'_p$ can be obtained by time integration of the acceleration signals with known initial values

$$\mathbf{V}'_p = \int_0^t \mathbf{a}'_p dt + \mathbf{V}'_p(t = 0). \tag{4}$$

There is, however, an additional complication since the accelerometers are fixed to the ship and are not vertically stabilized. The accelerometers do not directly measure an acceleration component $\mathbf{a}'$ but rather $\mathbf{a}_m = \mathbf{a}' - C\mathbf{g}$, where $\mathbf{a}_m$ is the output of the accelerometers, $\mathbf{g} = (0, 0, -g)$ is the acceleration due to gravity, and $C = T^{-1}$ is the inverse of the coordinate transformation matrix which is determined by the ship's attitude. This interaction turns out to be the most difficult problem in the fixed (strap-down) accelerometer ship-motion system. If we write Equation (3) at each accelerometer, it becomes a closed set of six equations due to the specific configuration of the accelerometer system. If we consider the difference of the velocities of the two accelerometers of each pair, the problem can be easily solved to obtain the angular velocity, attitude angles and the translational velocity. Finally, the corrected turbulent wind components can be obtained through Equation (1).

This correction procedure involves time integrations, which require the initial values of attitude angles $\phi(0), \theta(0)$ and $\psi(0)$ and the velocity $\mathbf{V}'_p(0)$. However, these initial data are not independently available for each data run, and they have to be obtained from assumed constraints on the ship motion. Since the time period of integration is as long as 24 minutes, with the ship anchored, it is plausible to assume that on average the mean attitude angles ϕ, θ and ψ and the angular velocity of the ship $\boldsymbol{\Omega}$ as well as the ship velocity $\mathbf{V}_{sh}$ are all zero. Therefore, we chose initial conditions such that the data-record mean values of ψ, θ, ψ, $\boldsymbol{\Omega}$ and $\mathbf{V}_{sh}$ are zero.

This correction scheme is based on the time integration of the acceleration signals from the six accelerometers, but it was found that the first integrals of the acceleration signals have large linear trends since each accelerometer has a small offset. Therefore, we high-pass filtered the acceleration signals before integration. As discussed earlier in this section, the calculation of attitude angles and angular velocities of the ship depends on the time integration of the differences of the two acceleration signals of each pair. The direct integrations of the acceleration differences of the two accelerometers of each pair are plotted in the top three panels (a, b, and c) in Figure 4, which show the linear trends. These integrations refer to the difference of velocity components of the two accelerometers of each pair in the direction to which they point. To avoid these trends, a high-pass filter was used on the sum and difference of the acceleration signals of the two accelerometers of each pair before they were integrated, and the corresponding integrations are shown in the bottom three panels (d, e, and f) in Figure 4. We explored varying the cutoff frequency, and found that 0.07 Hz removed the ship motion, while lower cutoff frequencies introduced anomalous peaks in the u and v spectra, as shown in Figure 5 for 0.02 Hz and 0.07 Hz together with the raw wind measurements. We have not investigated the reasons for the anomalous peaks in u and v spectra which occur for lower cutoff frequencies. For our experiments, the wind-correction scheme is applied with a high-pass filter of cutoff frequency 0.07 Hz.

4. Data Analysis

4.1. Ship Motion

As discussed in the last section, the ship motion can be determined through time integrations of the measured accelerations of the ship. Figure 6 shows a typical time series of the ship attitude angles, ϕ (roll), θ (pitch), and ψ (yaw), as well as the angular velocities $(\dot{\phi}, \dot{\theta}, \dot{\psi})$, obtained through integrations of the accelerations, from which the ship rotation with a swell-induced period of about 10 seconds can be seen clearly. For our experiments, it was found that $\psi < \theta < \phi$, since the ship was anchored.

The ship hull and superstructure may cause some flow distortion, and we chose to analyze only those cases when wind was onto the bow within $\pm 45°$, i.e., the distortion was assumed to be minimal.

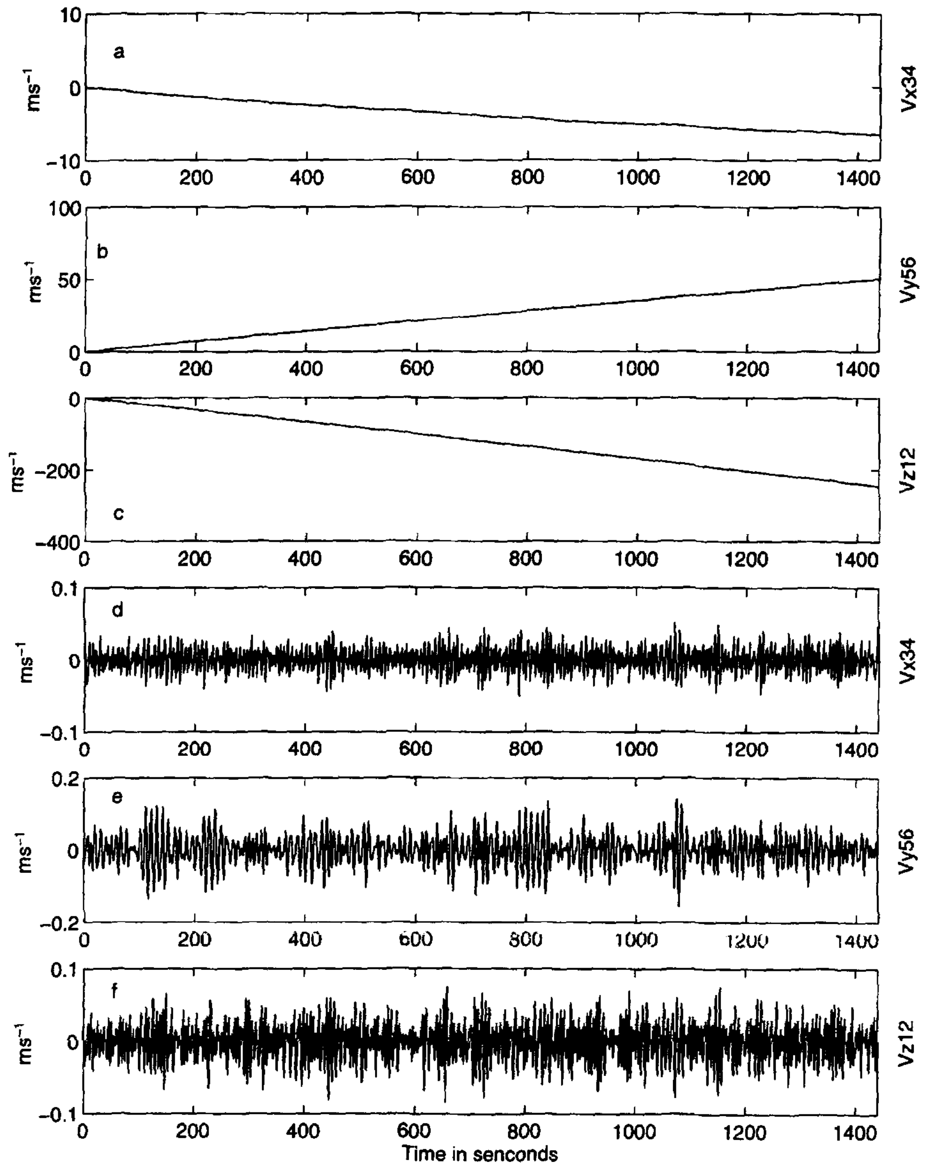

Figure 4. Time integrations of the differences between the two accelerometer signals of each pair before (a, b and c) and after (d, e, and f) a high-pass filter (0.07 Hz cutoff frequency) is applied to the signals. V_{z12} stands for the time integration of the difference between the accelerometers $a1$ and $a2$, V_{x34} for $a3$ and $a4$, and V_{y56} for $a5$ and $a6$, respectively.

4.2. Turbulent Wind Components

The raw measurements of turbulent wind components (especially the lateral and vertical components) were contaminated by the ship motion, as can be seen from

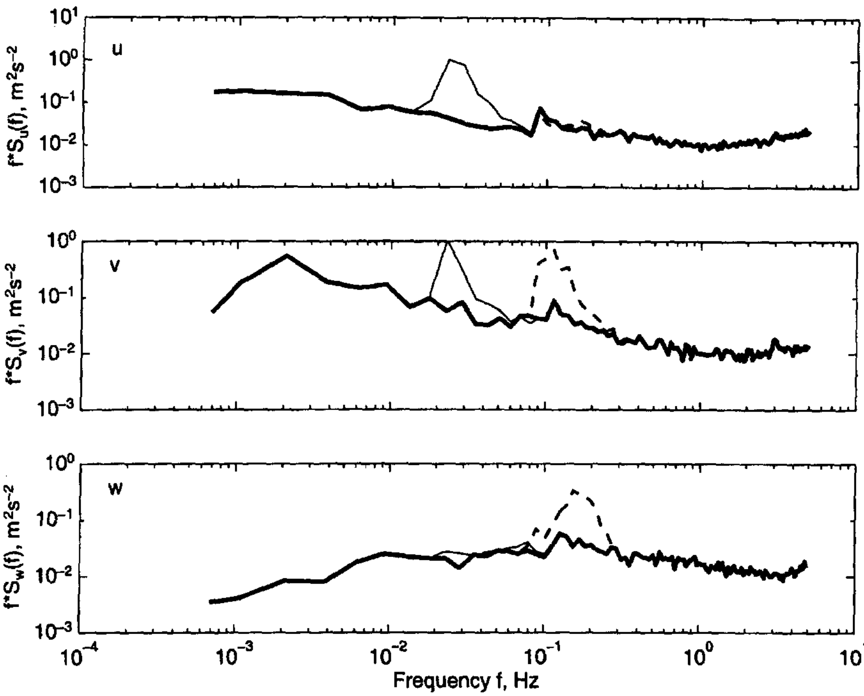

Figure 5. Power spectra of longitudinal (u), lateral (v) and vertical (w) wind components before (dashed lines) and after (solid lines) correction using high-pass filters with cutoff frequency of 0.02Hz (thin) and 0.07 Hz (thick) on the acceleration signals, respectively.

the time series in Figure 7 which shows an example of 100 seconds of wind components (longitudinal u, lateral v, and vertical w) in which wave-like motions of lower frequency embedded in the atmospheric turbulent fluctuations are visible (thin lines). The large low-frequency variations are considered to be due to the ship motion. The measurement of the longitudinal wind component was essentially not affected by the ship motion, while the lateral and vertical wind components were. The low-frequency contamination can also be seen in the power spectra in Figure 5 (dashed lines) which show the power spectral density of the 24-minute records of wind components, in which the dashed lines (raw measurements) show obvious peaks at the frequency around 0.1 Hz (0.08 to 0.3 Hz) which is the usual frequency range of ship motion contamination (Fujitani, 1985; Tsukamoto, *et al.*, 1990; Bradley, *et al.*, 1991). The power spectral density of the longitudinal component did not show an obvious peak in this frequency band. After correction for ship motion, the turbulent wind components are largely free from contamination with the wave-like motion eliminated in the time series (thick lines in Figure 7) and the spectral peaks removed in the frequency domain (thick solid lines in Figure 5).

As can be seen from Equation (1), the wind correction depends on the determination of the translational ($\mathbf{V}_{sh}$) and the rotational ($\boldsymbol{\Omega} \times T\mathbf{R}'$) components of

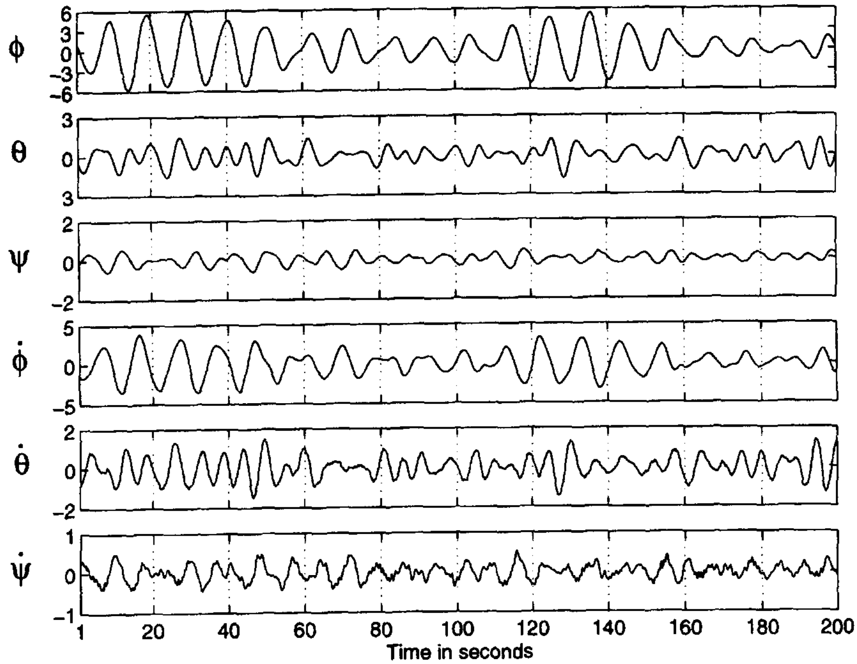

Figure 6. Time series of attitude angles (roll ϕ, pitch θ, and yaw ψ in degrees) and angular velocity ($\dot{\phi}, \dot{\theta}, \dot{\psi}$ in degrees/second) integrated from the acceleration signals observed at 13:00 (local time) November 25, 1992.

the ship motion. From the time series of these two components (Figure 8), it can be seen that for the vertical component, the translational motion (w_{sh}) has much more contribution to the correction than the rotational component (w_r) of the ship motion, while for the horizontal components, both the translational and rotational components of ship motion have equal importance in the correction.

The effect of the correction for ship motion can also be seen from the cospectra between the vertical component and the horizontal component of the turbulent wind measurements (Figure 9a; here the horizontal component is obtained by rotating the measured three wind components into the mean wind direction and zero-mean vertical wind of the 24-minute records). This correction is also shown in the cospectra between the vertical wind component and the fluctuating specific humidity from the Lyman-α (Figure 9b), but it is not as large as for the cospectra of wind components.

4.3. Specific Humidity and Virtual Temperature

The turbulent specific humidity q was obtained from the Lyman-α hygrometer which was operational during the first period of the observation but failed in the following two periods. Since an accurate calibration of the Lyman-α is essential for accurate latent heat flux determination, its nominal calibration was compared to the

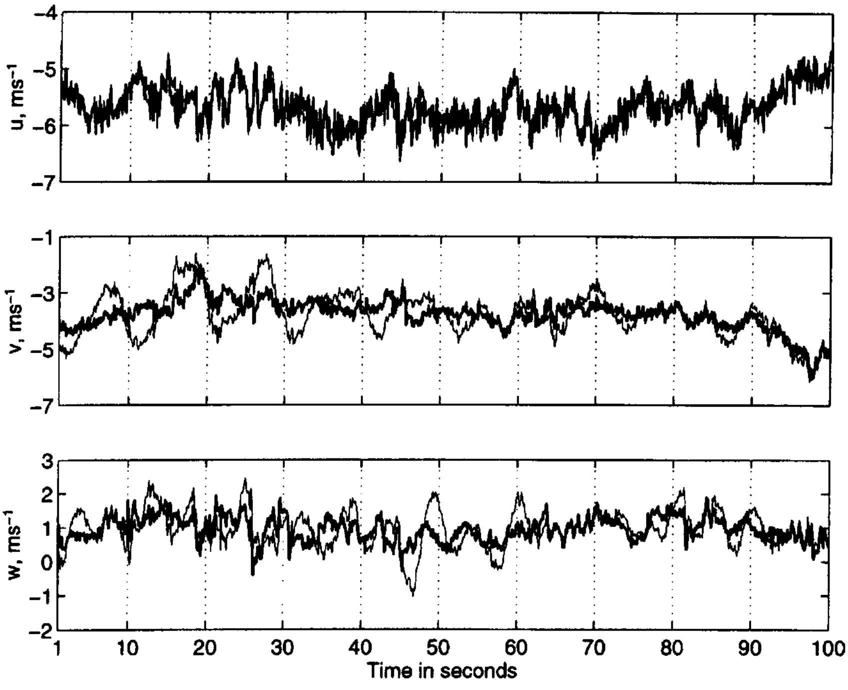

Figure 7. Time series of measured turbulent wind components (u, v and w, thin lines) and corresponding corrected wind components (thick lines). Data shown here is only 100 seconds of the whole run taken from 13:00 November 25, 1992.

ISS relative humidity data. The ISS sensor (Vaisala HMP35C) was on the top of the main mast which was about 60 metres aft of the Lyman-α hygrometer and about three metres higher. The specific humidity from the Lyman-α was averaged over one minute and compared with the 1-minute specific humidity values calculated from the ISS relative humidity, air temperature and air pressure measurements. The comparison of 14, 24-minute runs is shown in Figure 10, from which it can be seen that the sensitivity (slope) of the Lyman-α seems to be good, but there is a mean offset of 0.715 gkg^{-1}. Therefore, we accepted the nominal calibration slope of specific humidity q from the Lyman-α hygrometer.

The fluctuating virtual temperature was measured by the sonic anemometer-thermometer, but, unfortunately, the signal was unusable. Therefore, we were unable to calculate sensible heat flux from the eddy-correlation methods.

4.4. Spectral Results

After correction for ship motion, the three wind components are rotated into downstream (u), cross-stream (v) and vertical (w) components such that $\overline{v}$ and $\overline{w}$ are zero for the 24-minute data periods. The component $\overline{u}$ is in the direction of the mean wind. Hereafter, u, v and w represent the rotated downstream, cross-stream

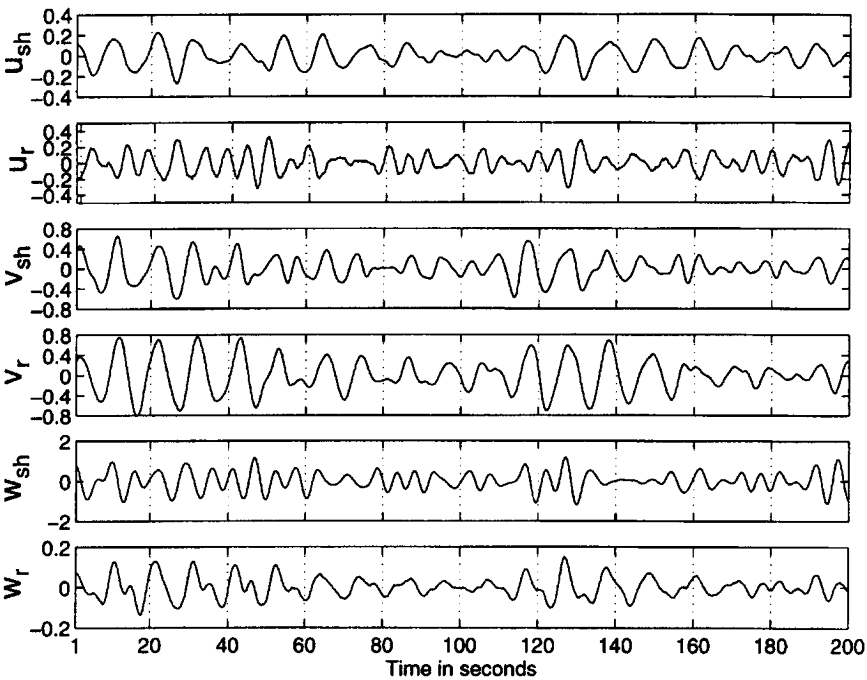

Figure 8. Translational ($\mathbf{V}_{sh}$) and rotational ($\mathbf{V}_r$) components of the ship motion (ms^{-1}). Run time is the same as in Figure 7.

and vertical wind components, respectively. To test the validity of the ship-board measurements, it is useful to compare spectra of u, v, w and q to those from previous experiments. Normalized spectra and cospectra from the R/V Kexue #1 data are compared with the overland results of Kaimal *et al.* (1972). Figure 11 shows the normalized power spectra of the vertical velocity component w and the downstream component u of the runs with stability parameter z/L varying from -0.02 to -7.94. In Figure 11, the solid lines are the Kaimal *et al.* (1972) curves and the numbers at the left end of the lines indicate the stability parameter z/L, where z is the measurement height and L is the Obukhov length (L is obtained from the bulk formula results). High frequency noise in the spectra is not plotted (Figures 11–13). The spectra show an inertial range at the high frequency end and vary with stability at lower frequency. Figure 12 shows the normalized spectra of the cross-stream component v and the specific humidity q. Again, the solid and dashed lines are the Kaimal *et al.* (1972) curves and the numbers indicate the stability parameter z/L. The spectra of the three wind components show general agreement with the results of Kaimal *et al.* (1972). The small peaks at the normalized frequency of around 0.2 might be due to residual ship motions which were not completely removed from the wind vector measurements. The cross-stream spectra are higher than those of Kaimal *et al.* at low frequencies (normalized frequency smaller than 0.004). The

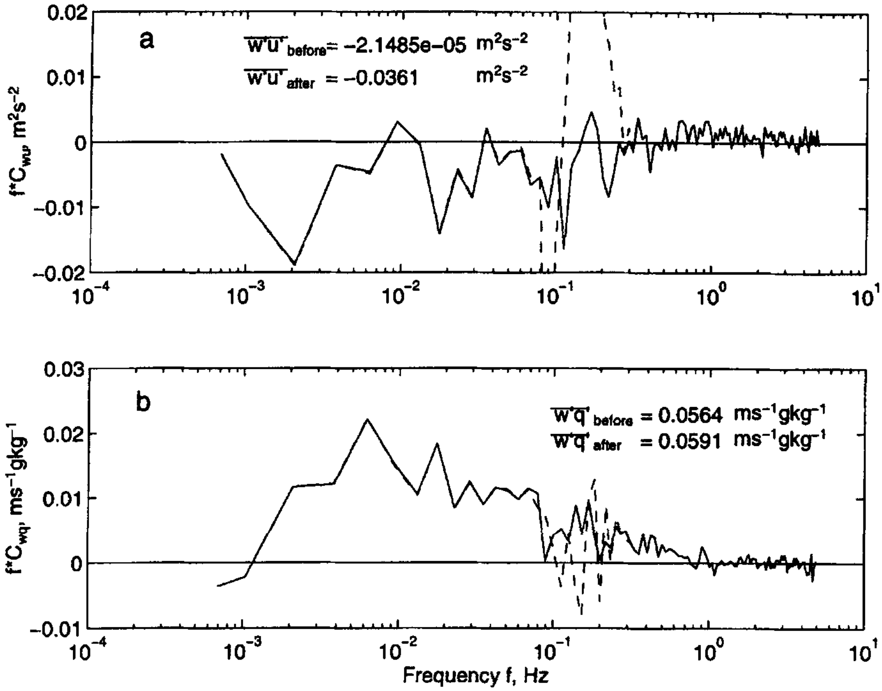

Figure 9. Cospectra between vertical component (w) of turbulent wind and (a) the horizontal component (u) of the turbulent wind, and (b) specific humidity (q) from Lyman-α. Solid lines are the cospectra of variables after correction for ship motion, and dashed lines before correction. The primes indicate fluctuation values. The time period is the same as in Figure 5.

solid lines in Figure 12b indicate the results for potential temperature fluctuations from Kaimal *et al.* (1972) which we take to be a surrogate for q, with the stability range of $-2.0 \leq z/L \leq 0$. At higher frequencies ($fz/U \geq 0.8$), normalized humidity spectra are smaller than, while at lower frequencies ($fz/U \leq 0.8$), humidity spectra are greater than, the Kaimal *et al.* (1972) potential temperature spectra. Earlier over-ocean measurements showed similar results (Schmitt *et al.* 1979). Figure 13 shows the $\overline{w'u'}$ and $\overline{w'q'}$ cospectra (hereafter the prime indicates the anomaly from its 24-minute mean). The momentum flux cospectrum is lower than that of Kaimal *et al.* in the range of $10^{-2} < fz/U < 0.5$. The $\overline{w'q'}$ cospectra fall off more rapidly than the predicted slope of $-\frac{4}{3}$. Schmitt *et al.* (1979) showed similar results from an over-land experiment (Schmitt *et al.*, 1979, Figure 9).

4.5. Momentum and Latent Heat Fluxes

Wind stress was estimated by both the TOGA COARE bulk formula (Fairall *et al.*, 1996) and an inertial dissipation method to compare with the stress computed by the eddy correlation method. For the eddy correlation method, the wind stress is calculated as $\tau = -\rho\overline{w'u'}$, where ρ is air density (1.15 kg m^{-3}), the primes

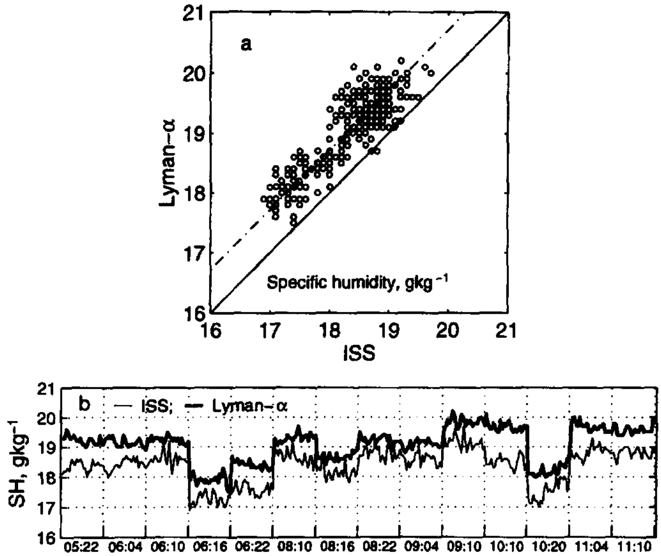

Figure 10. Comparison of specific humidity measurements from ISS and Lyman-α. (a) scatter plot, the dash-dotted line is 1:1 with offset 0.715 gkg^{-1}. (b) time series: each segment on x-axis represents one 24-minute run and the numbers on the bottom are the date (December 1992) and hour when the run started.

indicating the fluctuations. The bulk formula is $\tau = \rho C_D \overline{U}^2$ where the drag coefficient C_D is obtained by the TOGA COARE bulk formula (Fairall *et al.*, 1996) and $\overline{U}$ is wind speed from the ISS measurements as mentioned earlier. The inertial dissipation fluxes are calculated from turbulent structure functions by use of the modified TOGA COARE code written by Fairall and Coppin (1994, personal communication; cf. Fairall and Larsen, 1986). The results from this code are very close to those from the method of Anderson (1993).

For the eddy-correlation method, the wind stress is determined from the ogive of the cospectrum, which is the integral over all frequencies (from high frequency to low frequency) of cospectral intensity. The resulting ogive curve ideally should approach a constant value at low frequencies, indicating that all of the covariance has been "captured" (Friehe *et al.*, 1991). A sample cospectrum and ogive are shown in Figure 14, and the ogive shows the asymptotic approach to the constant value. For all runs, a judgment was made by inspecting the the ogives to determine the frequency band for the flux.

As mentioned at the beginning of this section, the sonic measurements of turbulent wind were possibly affected by the ship structure, depending on the wind direction relative to the ship coordinate system. The comparison of wind speeds measured at different locations of the ship may give an indication of the severity of flow distortion. Figure 15 shows the comparison of the ISS winds, whose sensor was located aft and higher than the sonic anemometer, and the sonic winds on the

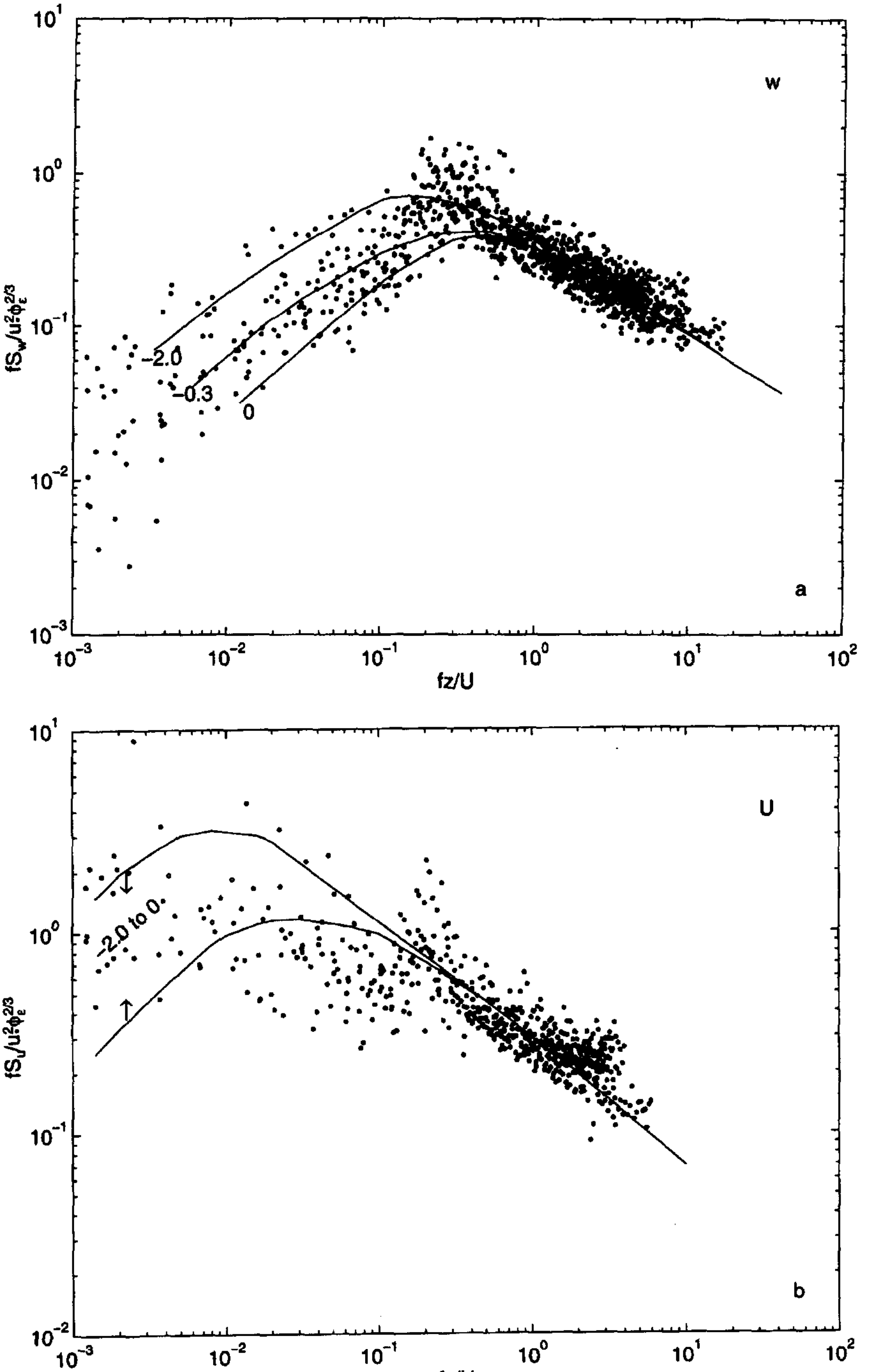

Figure 11. Normalized power spectra of (a) the vertical wind component w and (b) the downstream component u of typical runs with stability parameter z/L varying from -0.02 to -7.94. Here f is frequency in Hz, z measurement height, U mean wind speed, S_w the w power spectrum, u_* friction velocity and $\phi_\epsilon^{2/3}$ is the dimensionless dissipation rate of turbulent kinetic energy. The solid lines indicate the results from Kaimal *et al.* (1972) with different stabilities. Numbers at ends of lines indicate z/L values.

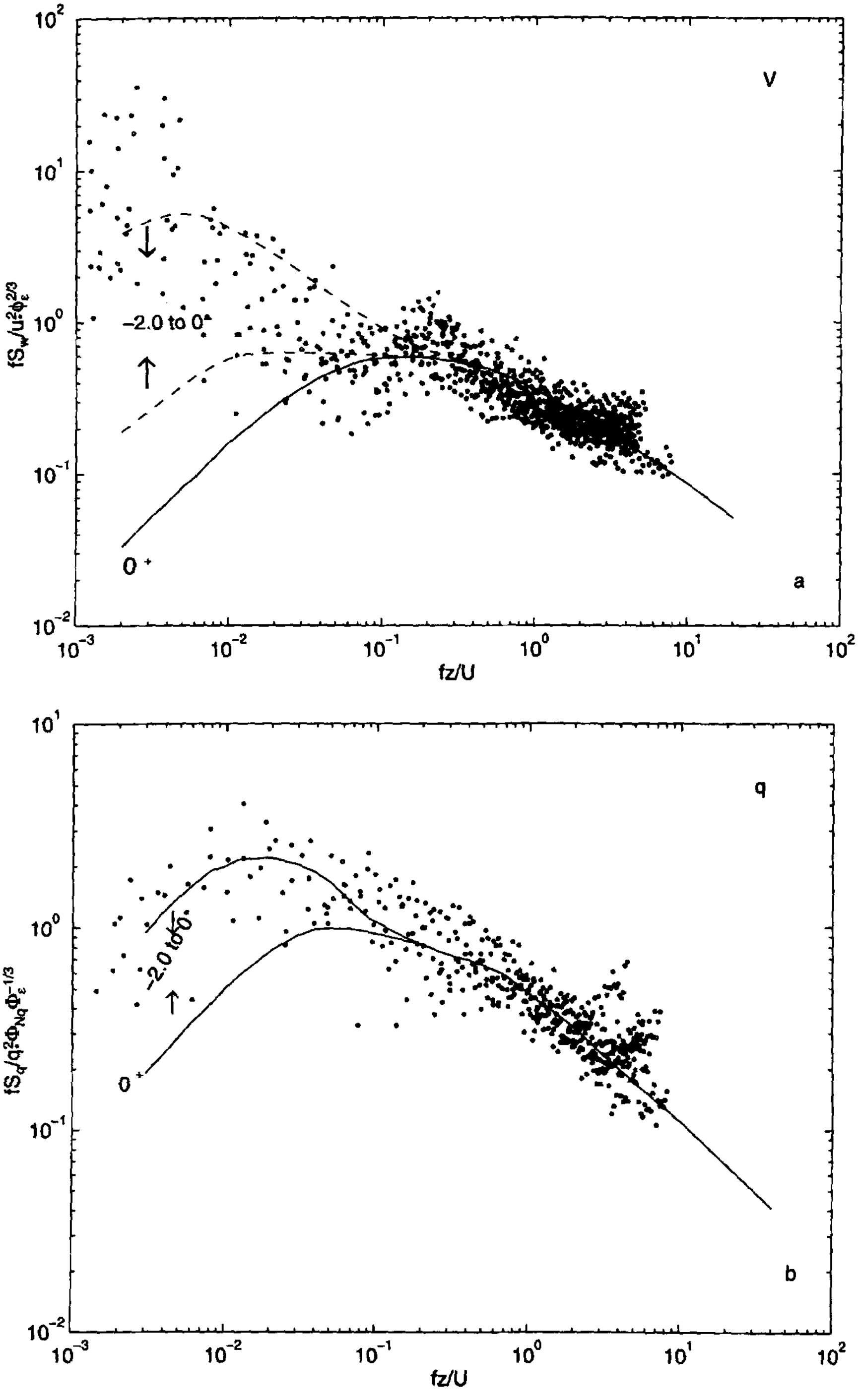

Figure 12. Normalized power spectra of (a) cross-stream component v and (b) the specific humidity q. The solid and dashed lines indicate the results from Kaimal *et al.* (1972). In the lower panel, the solid lines indicate the results for potential temperature from Kaimal *et al* (1972), which are taken to be a surrogate for specific humidity q.

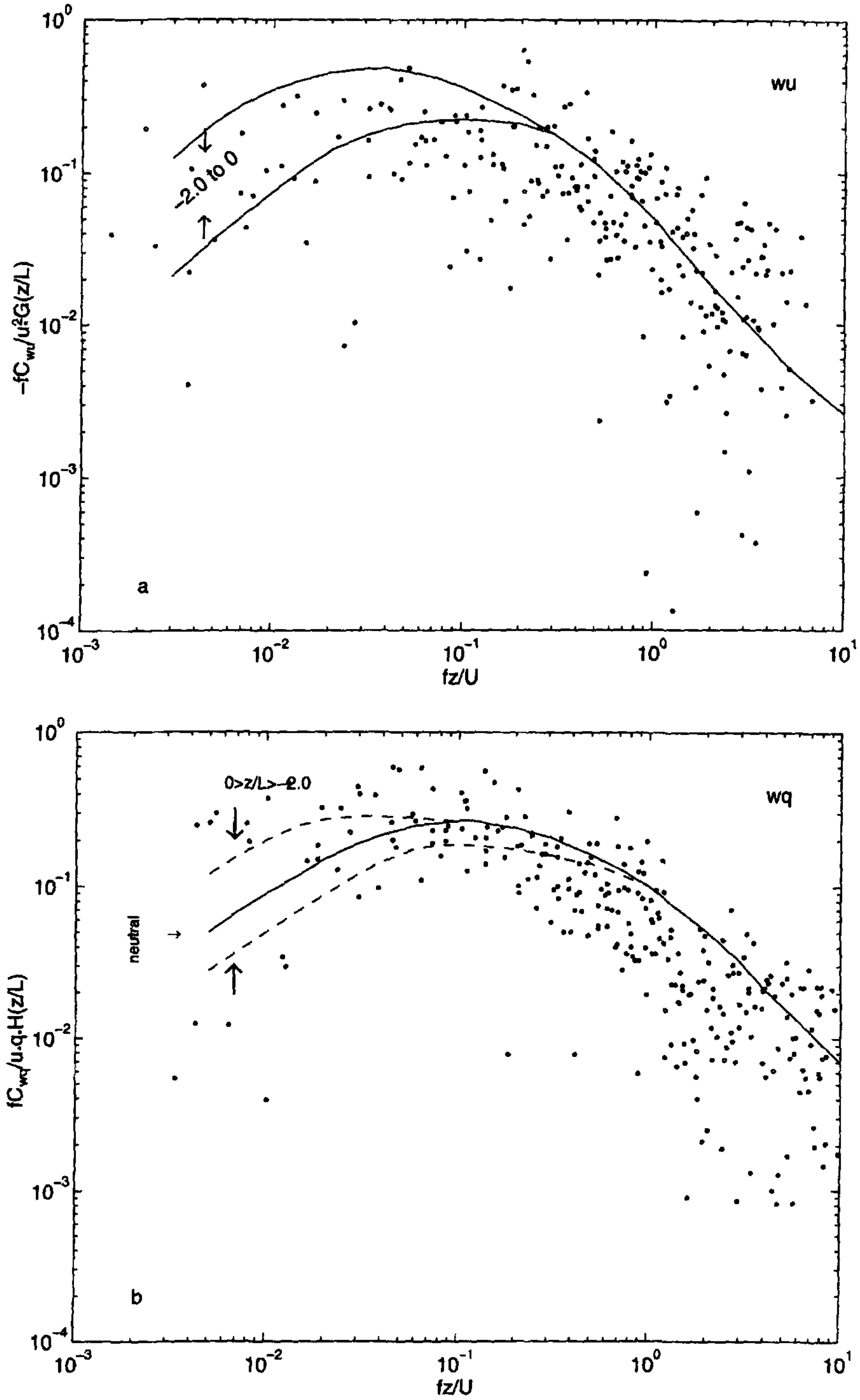

Figure 13. Normalized cospectra of vertical component and (a) downstream component ($w'u'$); and (b) specific humidity ($w'q'$). Solid lines indicate the results from Kaimal *et al.* (1972).

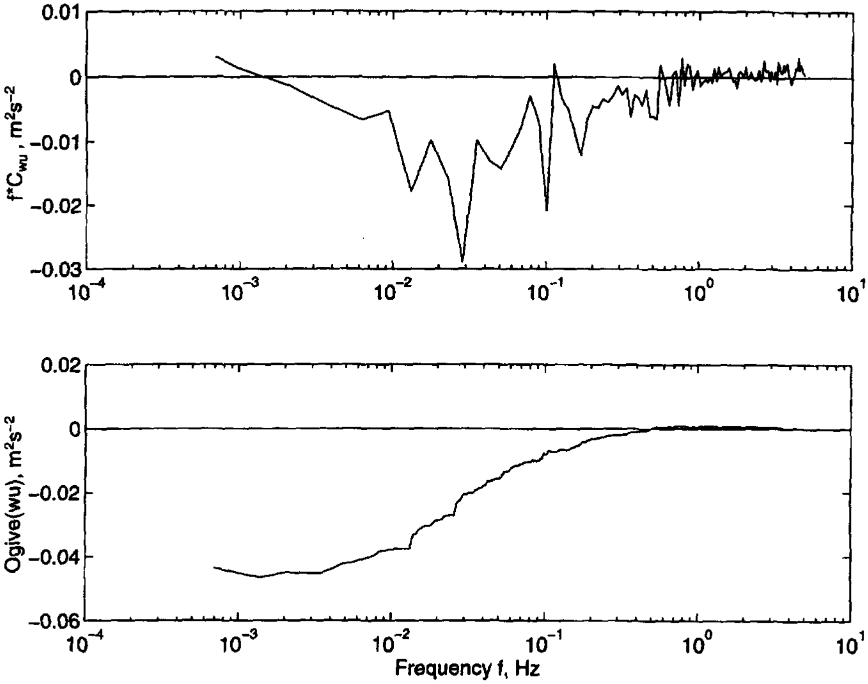

Figure 14. Cospectrum of vertical wind component w' and downstream wind component u' (upper); and the corresponding ogive (lower). Run time is 24 minutes starting from 16:00 February 2, 1993.

foremast. The agreement, for the 41 runs with wind within $\pm 45°$ of the bow, is good and perhaps indicates that gross flow distortion is not a major problem. The comparisons of wind stresses estimated from the ogive, bulk formula and inertial dissipation methods are also shown in Figure 15, from which it can be seen that the wind stresses from eddy correlation are smaller than those from the TOGA COARE bulk formula and inertial dissipation method, especially at higher wind speeds, while those from the bulk formula and the inertial dissipation method are, on average, in agreement. Flux data of several runs corrected for ship motion from R/V Franklin during the TOGA COARE IOP show similar results — the wind stresses from eddy correlation are smaller than those from the TOGA COARE bulk formula (Bradley, 1996, personal communication).

The cross-stream wind stress is $\tau_y = -\rho\overline{w'v'}$. Figure 16 shows the downstream (solid line) and cross-stream (dashed line) wind stresses, and it can be seen that the cross-stream values are not always zero, which means that the directions of the mean wind and stress may not be the same. In particular, both stress components were equal for Run 12 of Figure 16. Examination of the data for that run show that conditions were very non-stationary which may account for the observed behavior. In Runs 29-36, the cross-stream stress is finite and of opposite sign to the downstream stress. Conditions were close to stationary for these runs compared to Run

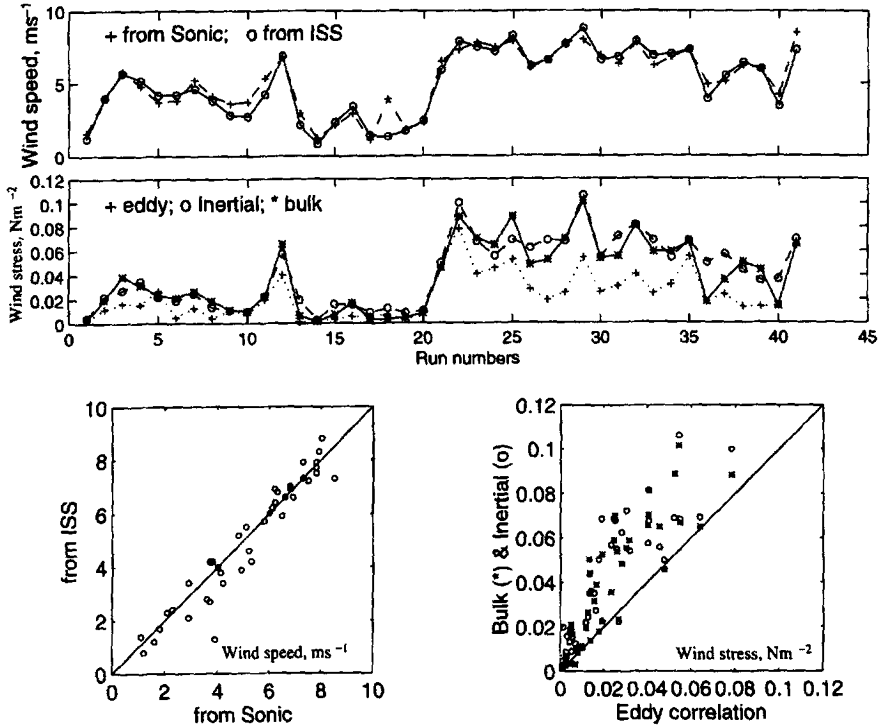

Figure 15. Comparison of wind speeds from ISS and sonic anemometer (top and bottom-left panels); And comparison of wind stress estimated by bulk formula (*), inertial (o) dissipation and by eddy correlation (+) (middle and bottom-right panels).

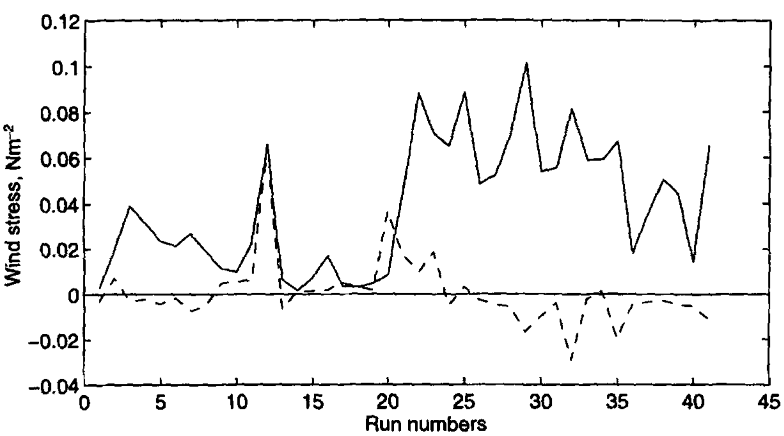

Figure 16. Downstream (solid line) and cross-stream (dashed line) wind stresses computed by eddy correlation from sonic anemometer measurements.

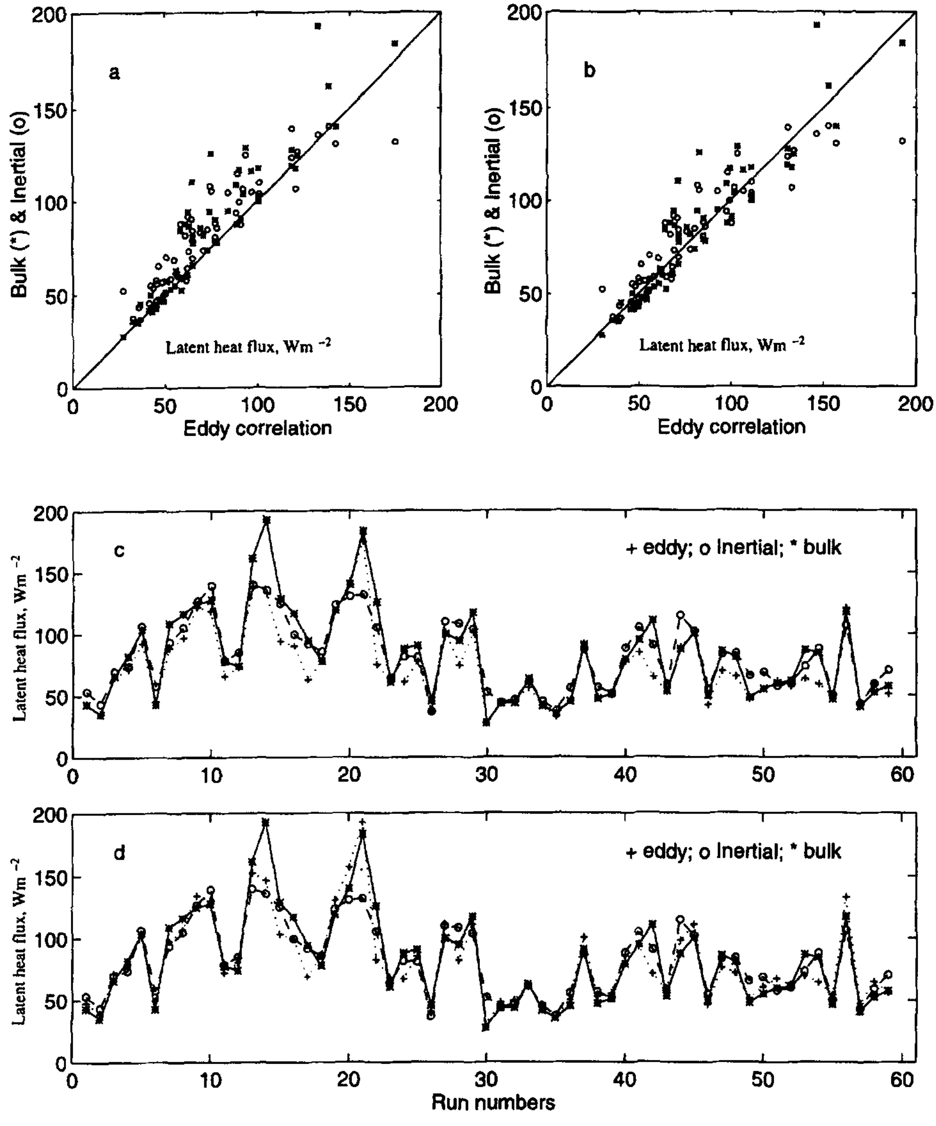

Figure 17. Comparison of latent heat fluxes estimated by three different methods, eddy correlation (+), TOGA COARE bulk formula (*) and inertial dissipation (*o*). The eddy correlation latent heat flux values in panels *a* and *c* were computed directly from the ogives, while in panels *b* and *d* were adjusted by plus 10% because of the sensor separation.

12, and the cospectra showed that generally there were finite cross-stream stress contributions over a wide range of frequencies, similar to those for the downstream stress cospectra. Misalignment of wind stress and wind direction over the ocean has been observed before in measurements by Geernaert (1988) and Rieder *et al.* (1994).

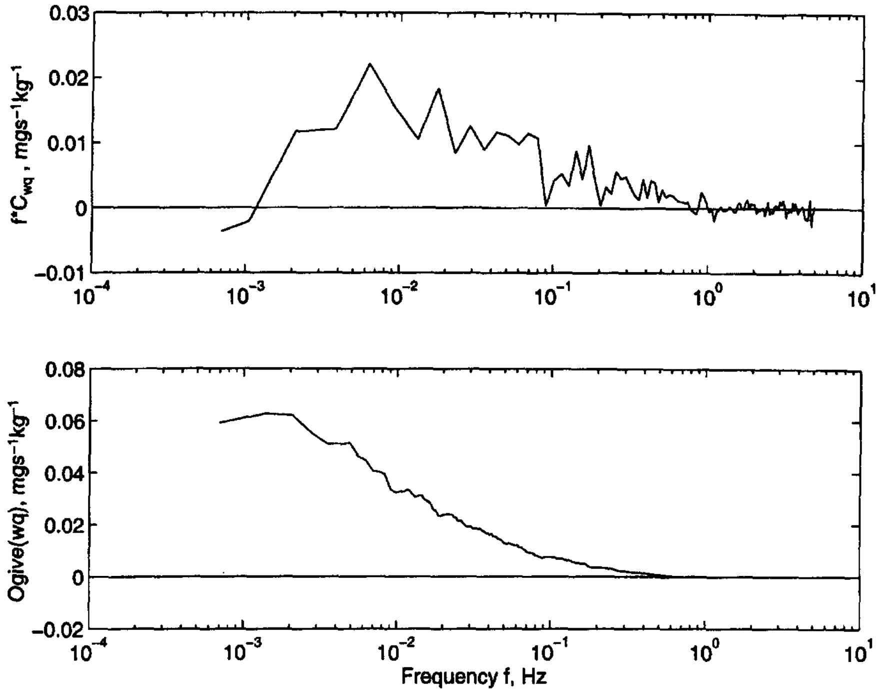

Figure 18. Cospectrum and ogive of vertical wind component w' and specific humidity q'. Run time starting from 13:00 November 25, 1992.

The latent heat flux was calculated as $\rho L_e \overline{w'q'}$, where L_e is latent heat (2433.6 $\mathrm{Jg^{-1}}$) and q' is the specific humidity fluctuation (in $\mathrm{gkg^{-1}}$). As described in the previous section, high frequency specific humidity data were only available for the first period of the IOP. The comparison of latent heat fluxes by eddy correlation, the TOGA COARE bulk formula (Fairall *et al.*, 1996) and inertial dissipation (Fairall and Larsen, 1986) methods is shown in Figure 17. It can be seen that the latent heat flux values from the different methods are in closer agreement than for momentum flux. The eddy correlation latent heat flux values in panel *a* and *c* in Figure 17 were computed from the ogives without adjustment for the horizontal separation of the wind sensor and humidity sensor, while the values in panel *b* and *d* were adjusted by plus 10% because of the sensor separation, as suggested in Moore (1986) and Lee and Black (1994). After this adjustment, the latent heat flux values from the three different methods are in better agreement. For eddy correlation, the latent heat flux was determined from the ogives of vertical wind component w' and specific humidity q', similar to momentum flux. A sample cospectrum and ogive of w' and q' flux are shown in Figure 18.

The turbulent heat transfer coefficient C_e (upper panel in Figure 19) determined from the eddy correlation latent heat flux shows an increase with decreasing wind speed for the wind speeds lower than 2 $\mathrm{ms^{-1}}$ and is almost constant for wind

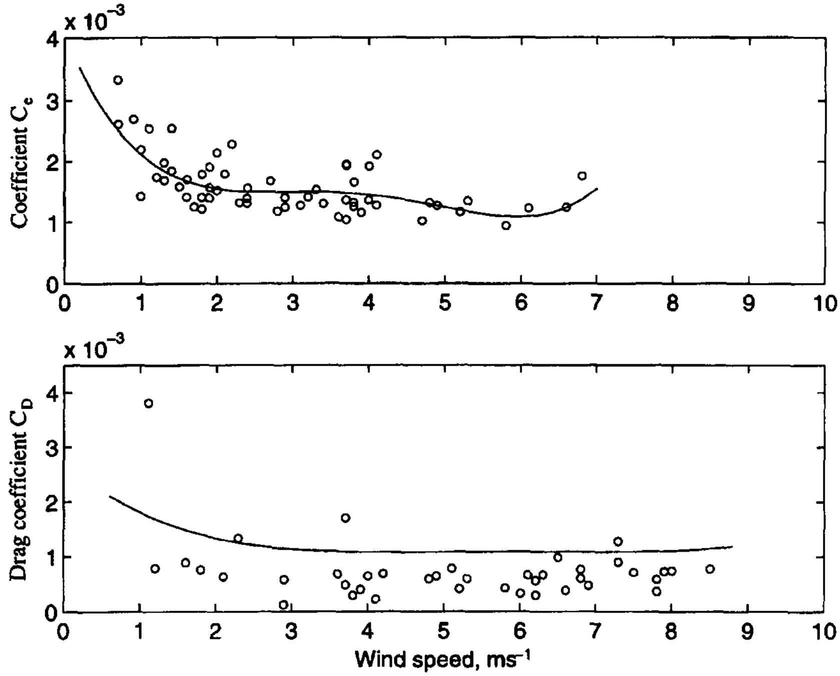

Figure 19. Turbulent transfer coefficient for latent heat (C_e, upper panel) and drag coefficient (C_D, lower panel) derived from eddy correlation fluxes (o) and that used for the TOGA COARE bulk formula (solid line, Fairall, *et al.*, 1996).

speeds higher than 2 ms^{-1}. The present values of C_e agree well with that used for the TOGA COARE bulk algorithm (Fairall et al., 1996), as shown in Figure 19. The drag coefficient C_D (lower panel in Figure 19) is lower than that of the TOGA COARE bulk algorithm, but has the same tendency of slightly increasing with wind speed for the wind speeds higher than 3 ms^{-1}. For the wind speeds lower than 3 ms^{-1}, unfortunately, there are only a few data available, and only one data point shows the increase of C_D at low wind speed.

5. Discussion and Conclusions

The analysis of the data from R/V Kexue #1 shows that the strap-down six accelerometer system can be used to remove most of the ship motion at the wave-induced frequency band from the measured sonic anemometer signals provided the accelerometer signals are high-pass filtered to remove offsets. For TOGA COARE, the ship was anchored and the main motion contamination was in the vertical and transverse wind components; the component along the longitudinal axis of the ship did not exhibit much contamination. Data reduction was limited to wind directions within ±45° of the bow; comparison of wind speeds from the sonic anemometer on the foremast and an ISS sensor aft were good, indicating no gross flow distortion.

The motion-corrected turbulence measurements gave latent heat eddy correlation flux values which compared reasonably well with those estimated from the TOGA COARE bulk formula and inertial dissipation rate techniques. The latent heat cospectra did not exhibit significant motion contamination. However, the eddy correlation wind stress values were lower than those predicted by the TOGA COARE bulk formula and inertial dissipation rate techniques. The reasons for this are not known at present; flow distortion of the turbulent wind field around the bow of the ship could be a possibility. However, the spectral characteristics of the velocity components and humidity, stress and latent heat flux agreed reasonably well with those obtained over land and, in detail, with some previous results in the marine surface layer.

The six accelerometer system appears to be relatively robust for use at sea for extended periods. The quality of the accelerometers and their accurate installation and calibration are important factors to ensure good calculated motion variables. Some of the problems may be overcome by filtering the accelerometer signals as we have done, although the results appear to be quite sensitive to the cut-off frequency used. A thorough investigation of the reason for the sensitivity to the filter cutoff needs to be performed. The increased availability of GPS for platform attitude and velocity determination since TOGA COARE may be a good supplement to the accelerometer technique.

Acknowledgements

X. Song and D. Hu thank Profs. Yongping Zhao and Yongli Chen and senior engineers Aiqing Lu and Yatian Huang from the Institute of Oceanology, Chinese Academy of Sciences, who were in charge of instrument installation and data acquisition during the field experiment. We are also most grateful to the officers and crew of R/V Kexue #1 for their efforts. X. Song thanks Drs. Djamal Khelif and Perry Fuehrer, and Sean Burns, Scott Miller, Brad Berger, and Dr. Frank Bradley for their helpful discussion and comments. We also thank the TOGA COARE International Project Office staff for their help in the field experiment. This work was supported by the Chinese Academy of Sciences, US NSF and NOAA OGP. We are also grateful for the comments of the two anonymous reviewers.

References

Anctil, F., Donelan, M. A., Drennan, W. M., and Graber, H. C.: 1994, 'Eddy-Correlation Measurements of Air-Sea Fluxes from a Discus Buoy', *J. Atmos. Ocean. Tech.* **11**, 1144–1150.

Anderson, R. J.: 1993, 'A Study of Wind Stress and Heat Flux over the Open Ocean by the Inertial-Dissipation Method', *J. Phys. Ocean.* **23**, 2153–2161.

Bradley, E. F., Coppin, P. A., and Godfrey, J. S.: 1991, 'Measurements of Sensible and Latent Heat Flux in the Western Equatorial Pacific Ocean', *J. Geophys. Res.* **96**(supplement), 3375–3389.

Bradley, E. F. and Weller, R. (editors): 1995, 'Third Workshop of the TOGA COARE Air-Sea Interaction (Flux) Working Group', East-West Center, University of Hawaii, Honolulu USA, 2–4 August 1995.

Fairall, C. W., and Larsen, S. E.: 1986, 'Inertial Dissipation Methods and Turbulent Fluxes at the Air-Ocean Interface', *Boundary-Layer Meteorol.* **34**, 287–301.

Fairall, C. W., Bradley, E. F., Rogers, D. P., Edson, J. B., and Young, G. S.: 1996, 'Bulk Parameterization of Air-Sea Fluxes for Tropical Ocean Global Atmosphere Coupled Ocean Atmosphere Response Experiment', *J. Geophys. Res.* **101**, 3747–3764.

Friehe, C. A., Shaw, W. J., Rogers, D. P., Davidson, K. L., Large, W. G., Stage, S. A., Crescenti, G. H., Khalsa, S. J. S., Greenhut, G. K., and Li, F.: 1991, 'Air-Sea Fluxes and Surface Layer Turbulence around a Sea Surface Temperature Front', *J. Geophys. Res.* **96**, 8593–8609.

Fujitani, T.: 1985, 'Method of Turbulent Flux Measurement on a Ship by Using a Stable Platform System', *Papers in Meteorol. and Geophys.* **36**, 157–170.

Geernaert, G. L.: 1988, 'Measurements of the Angle between the Wind Vector and Wind Stress Vector in the Surface Layer over the North Sea', *J. Geophys. Res.* **93**, 8215–8220.

Kaimal, J. C., Wyngaard, J. C., Izumi Y., and Cote, O. R.: 1972, 'Spectral Characteristics of Surface-layer Turbulence', *Quart. J. Roy. Meteorol. Soc.* **98**, 563–589.

Lee, X. and Black, T. A.: 1994, 'Relating Eddy Correlation Sensible Heat Flux to Horizontal Sensor Separation in the Unstable Atmospheric Surface Layer', *J. Geophys. Res.* **99**, 18545–18553.

Miller, M. J., Beljaars, A. C. M., and Palmer, T. N.: 1992, 'The Sensitivity of the ECMWF Model to the Parameterization of Evaporation from the Tropical Oceans', *J. Climate* **5**, 418–434.

Mitsuta, Y. and Fujitani, T.: 1974, 'Direct Measurement of Turbulent Fluxes on a Cruising Ship', *Boundary-Layer Meteorol.* **6**, 203-217.

Moore, C. J.: 1986, 'Frequency Response Correction for Eddy Correlation Systems', *Boundary-Layer Meteorol.* **37**, 17–35.

Rieder, K. F., Smith, J. A., and Weller, R. A.: 1994, 'Observed Directional Characteristics of the Wind, Wind Stress and Surface Wave on the Open Ocean', *J. Geophys. Res.* **99**, 22589–22596.

Schmitt, K. F., Friehe, C. A., and Gibson, C. H.: 1979, 'Structure of Marine Surface Layer Turbulence', *J. Atmos. Sci.* **36**, 602–618.

Shao, Y.: 1995, 'Correction of Turbulent Wind by Measurements Contaminated by Irregular Motion of a Ship – TOGA COARE Project', CSIRO Center for Environmental Mechanics, Canberra, Australia, *Technical Report* No. 70, March 1995.

Tsukamoto, O., Ohtaki, E., Ishida, H., Horiguchi, M., and Mitsuta, Y.: 1990, 'On-Board Direct Measurements of Turbulent Fluxes over the Open Sea', *J. Meteorol. Soc. Japan* **68**, 203–211.

Tsukamoto, O. and Ishida, H.: 1995, 'Turbulent Flux Measurements and Energy Budget Analysis over the Equatorial Pacific during TOGA-COARE IOP', *J. Meteorol. Soc. Japan* **73**, 557–568.

Webster, P. J. and Lukas, R.: 1992, 'TOGA COARE: The Coupled Ocean-Atmosphere Response Experiment', *Bull. Amer. Meteorol. Soc.* **73**, 1377–1416.